Biophysical Journal Volume 107 December 2014 2872–2880

Article

The Motility of Axonemal Dynein Is Regulated by the Tubulin Code

Joshua D. Alper,[1,2] Franziska Decker,[2] Bernice Agana,[1,2] and Jonathon Howard[1,2,*]
[1]Department of Molecular Biophysics and Biochemistry, Yale University, New Haven, Connecticut; and [2]Max Planck Institute of Molecular Cell Biology and Genetics, Dresden, Germany

ABSTRACT Microtubule diversity, arising from the utilization of different tubulin genes and from posttranslational modifications, regulates many cellular processes including cell division, neuronal differentiation and growth, and centriole assembly. In the case of cilia and flagella, multiple cell biological studies show that microtubule diversity is important for axonemal assembly and motility. However, it is not known whether microtubule diversity directly influences the activity of the axonemal dyneins, the motors that drive the beating of the axoneme, nor whether the effects on motility are indirect, perhaps through regulatory pathways upstream of the motors, such as the central pair, radial spokes, or dynein regulatory complex. To test whether microtubule diversity can directly regulate the activity of axonemal dyneins, we asked whether in vitro acetylation or deacetylation of lysine 40 (K40), a major posttranslational modification of α-tubulin, or whether proteolytic cleavage of the C-terminal tail (CTT) of α- and β-tubulin, the location of detyrosination, polyglutamylation, and polyglycylation modifications as well as most of the genetic diversity, can influence the activity of outer arm axonemal dynein in motility assays using purified proteins. By quantifying the motility with displacement-weighted velocity analysis and mathematically modeling the results, we found that K40 acetylation increases and CTTs decrease axonemal dynein motility. These results show that axonemal dynein directly deciphers the tubulin code, which has important implications for eukaryotic ciliary beat regulation.

INTRODUCTION

The tubulin code hypothesis proposes that microtubule diversity differentially regulates molecular motors and microtubule associated proteins (1). Microtubule diversity arises through the expression of multiple tubulin isotypes, which differ primarily in their C-terminal tails (CTTs) (2), and through multiple posttranslational modifications (PTMs) (2–4). These include acetylation of α-tubulin's lysine 40 (K40) on the luminal surface of the microtubule and modifications to the α- and β-tubulin CTTs (2) on the outer surface of the microtubule. However, the molecular mechanisms by which the tubulin code regulates cellular processes are only just beginning to be understood.

There is cell biological and genetic evidence that tubulin PTMs regulate the activity of molecular motors in the cytoplasm. For example, K40 acetylation marks stable microtubules, which preferentially recruit cytoplasmic dynein and kinesin-1, and increases the speed of kinesin-1 (5–7); this is thought to play an important role in neuronal polarization (8) and integrity (5,9). To test whether motors can directly sense tubulin modifications, the recent identification of PTM enzymes, including α-tubulin acetyltransferase (αTAT) (10,11) and SIRT2 (12), has facilitated biochemical studies. In the case of K40 acetylation, no effect on the motility of kinesin-1 was found using purified proteins (13,14), suggesting that regulation of kinesin-1 motility by acetylation may be indirect. On the other hand, in vitro assays show that CTTs and their associated PTMs can regulate a variety of cytoplasmic motors (15), extending earlier studies showing that enzymatic removal of the CTTs can influence the processivity and microtubule binding rate of kinesin-1, kinesin-13, and cytoplasmic dynein (16–19). Thus, there is evidence that PTMs can directly regulate cytoplasmic motor motility.

Cilia and flagella are motile and sensory organelles containing an axoneme, a microtubule-based structure. Axonemal microtubules are distinguished from cytoplasmic microtubules through the differential expression of tubulin isotypes and prominent PTMs (4), suggesting that microtubule diversity may play a role in ciliary function. Indeed, K40 acetylation defects slightly reduce the swimming speed of *Chlamydomonas* cells (20) and cause abnormal mouse sperm function (21), though no swimming defects are seen in *Tetrahymena* cells (22). Defects in polyglutamylation, the addition of glutamic acid side chains to CTTs (23), slow *Tetrahymena* (24) and *Chlamydomonas* (25,26) swimming and reduce mouse brain ependymal cilia beat frequency (27). Antibodies against the CTT sequences of β-I, β-IV, and β-V tubulin, which are cilia and flagella specific isotypes (2), but not against other tubulin sequences, inhibit the beating of bovine cilia (28). Because these effects

Submitted July 22, 2014, and accepted for publication October 22, 2014.

*Correspondence: jonathon.howard@yale.edu

Bernice Agana's present address is Chemistry Department, Missouri State University, Springfield, Missouri.

Editor: Kazuhiro Oiwa.

0006-3495/14/12/2872/9 $2.00

http://dx.doi.org/10.1016/j.bpj.2014.10.061

occur without causing structural defects to the axoneme (21,22,25), it is possible that the tubulin code regulates axonemal dynein, the motor protein that is directly responsible for ciliary motility. However, to our knowledge, there is no direct, in vitro evidence of axonemal dynein regulation through tubulin diversity. In this study, we present biochemical and biophysical evidence that axonemal dynein can read the tubulin code.

MATERIALS AND METHODS

Cells and media

As described in previous works (29,30), the *Chlamydomonas reinhardtii* strain used was *oda2-t-lc2-bccp* (31), which lacks the γ HC outer arm axonemal dynein motor and has a light-chain 2 biotin-carboxyl-carrier protein (lc2-bccp) construct to bind the α and β HC outer arm axonemal dynein complexes to a streptavidin-coated substrate in a site-specific manner (31). Outer arm axonemal dyneins were used in these studies because their activity has been associated with establishing ciliary beat frequency (32), and PTM mutants often have beat frequency phenotypes (25,27). The cells were grown in liquid Tris-acetate-phosphate (TAP) medium (20 mM Tris, 7 mM NH_4Cl, 0.40 mM $MgSO_4$, 0.34 mM $CaCl_2$, 2.5 mM PO_3^{-4}, and 1000-fold diluted Hutner's trace elements (33), titrated to pH 7.0 with glacial acetic acid) with continuous aeration and 24 h of light at room temperature. 60 L of cell culture were grown to a density of 5 to 10×10^6 cells/mL.

Axonemal dynein purification

As described in previous work (29,30), the *oda2-t-lc2-bccp* cells were harvested and the axonemes were isolated by standard methods (34). Briefly, cells were harvested by centrifugation and deciliated with dibucaine (Sigma-Aldrich, St. Louis, MO). The cilia were isolated and diluted into HMDE (30 mM HEPES, 5 mM $MgSO_4$, 1 mM DTT, and 1 mM EGTA, titrated to pH 7.4 with potassium hydroxide (KOH)) with 0.4 mM Pefabloc (Sigma-Aldrich). They were demembranated with IGEPAL CA-630 (Sigma-Aldrich) and washed in HMDE. The axonemal dyneins were extracted with 0.6 M KCl and purified using a MonoQ 10/100 GL (GE Healthcare, Piscataway, NJ) ion-exchange column (35). The axonemal dyneins were eluted with a linear gradient of 150 to 400 mM KCl in HMDE and stored at 300 μg/mL in 30% saturated sucrose at -80°C.

Tubulin purification and labeling

Porcine brain tubulin was purified by standard methods (36). Briefly, porcine brains were homogenized and clarified by centrifugation. Active tubulin in the supernatant was purified with polymerization and depolymerization cycles. Tubulin was separated from the microtubule-associated proteins with a phosphocellulose column (P11, Whatman, Piscataway, NJ). Porcine brain tubulin was labeled with 5 (and 6)-carboxytetramethylrhodamine, succinimidyl ester (TAMRA, SE; Invitrogen, Life Technologies, Darmstadt, Germany) by incubating the dye with polymerized microtubules. The active labeled tubulin was obtained with additional polymerization and depolymerization cycles.

Axonemal tubulin from *Chlamydomonas* was purified as previously described (29,30). Briefly, the microtubules in the axoneme pellet obtained after axonemal dynein extraction were induced to depolymerize with 50 mM $CaCl_2$ and incubation in an ice-cold sonicating bath. This crude tubulin extract applied to a TOG1/2 domain column (37), and eluted with KCl.

Microtubule preparation

Rhodamine-labeled porcine brain microtubules were polymerized from 2 to 8 μM tubulin, 30% rhodamine-labeled and 70% unlabeled, in BRB80 (80 mM PIPES, 1 mM $MgCl_2$, and 1 mM EGTA, titrated to pH 6.9 with KOH) with 1 mM Guanosine-5′-[(α,β)-methyleno]triphosphate (GMPCPP, Jena Bioscience, Jena, Germany), and 1 mM $MgCl_2$, for 2 h at 37°C. They were stabilized by diluting them in BRB80 with 20 μM taxol (paclitaxel, Sigma-Aldrich).

Chlamydomonas microtubules were polymerized from 8 μM tubulin in BRB80 with 4 mM $MgCl_2$, 1 mM GTP, and 4% DMSO for 30 min at 37°C. They were stabilized by diluting them in BRB80 with 20 μM taxol.

In vitro acetylation and deacetylation

To acetylate microtubules in vitro (13), 20 μM 30% rhodamine-labeled porcine microtubules were incubated with 3 μM αTAT (recombinantly expressed and purified murine αTAT, which is also known as MEC-17 (10), was a generous gift from Wilhelm Walter and Stefan Diez, B CUBE–Center for Molecular Bioengineering, TU Dresden, Dresden, Germany) and 120 μM acetyl-coenzyme A (acetyl-CoA, Sigma-Aldrich) in 60 mM Tris-HCl, pH 8.0 for the indicated times at 28°C.

To deacetylate microtubules in vitro, *Chlamydomonas* tubulin at 17 μM was incubated with 50 μg/mL human recombinant His-Tag SIRT2 (EMD Millipore, Darmstadt, Germany), 0.5 mM NAD+ (Sigma Aldrich) in 40 mM PIPES with 0.5 mM DTT, 0.8 mM EGTA, and 0.5 mM $MgSO_4$ at pH 7.0 at room temperature for 2 h. This deacetylated tubulin was further polymerized into microtubules as described above.

The controls for both cases were treated in the same manner, just without addition of αTAT or SIRT2. The microtubules were used for gliding assays, SDS-PAGE, and Western blots.

CTT cleavage

Forty μM microtubules were incubated with 10 μg/mL or 200 μg/mL subtilisin A (Sigma-Aldrich) in BRB80 with 20 μM taxol at 30°C for 1 h. The reaction was quenched by addition of 4 mM phenylmethylsulfonyl fluoride (Thermo Scientific). The s-tubulin microtubules were separated from the cleaved CTTs and the buffer was exchanged to BRB80 with 20 μM taxol by centrifugation in an Airfuge Air-Driven Ultracentrifuge (Beckman Coulter, Brea, CA). The controls were treated in the same manner, just without the addition of subtilisin A.

SDS-PAGE, Western blots, and antibodies

SDS-PAGE was done using 4-12% Bis-Tris gels (NuPAGE, Life Technologies, Darmstadt, Germany) or 4%–15% Mini-PROTEAN TGX Stain-Free Gels (BioRad, Hercules, CA). Proteins were visualized with Coomassie brilliant blue (Life Technologies) or by following the manufacturers instructions for visualizing stain-free gels using the ChemiDoc MP gel imaging system (BioRad). Proteins were transferred to nitrocellulose membranes with an iBlot (Life Technologies) or a TurboBlot (BioRad).

Primary antibodies were used to detect particular tubulin motifs: K40 acetylation was detected with anti-K40 acetylated α-tubulin (6-11B-1, Sigma-Aldrich); polyglutamylation was detected with antipolyglutamylated tubulin (GT335, AdipoGen, San Diego, CA); detyrosination was detected with antidetyrosinated tubulin (AB3201, EMD-Millipore); Δ2 tubulin was detected with anti-Δ2 tubulin (Δ2, EMD-Millipore); α-tubulin CTTs were detected with anti-α-tubulin YL1/2 (MAB1864, EMD-Millipore); β-tubulin CTTs were detected with anti-β-III tubulin (TU-20, Santa Cruz Biotechnology, Dallas, TX); non-CTT epitopes of α-tubulin were detected with anti-α-tubulin (DM1-α, Sigma-Aldrich); and non-CTT epitopes of β-tubulin were detected with anti-β-tubulin (TU-06, EXBIO, Vestec, Czech Republic). Appropriate alkaline-phosphatase conjugated

secondary antibodies (goat, mouse, or rabbit; Sigma-Aldrich and Life Technologies) were used with NBT/BCIP (WesternBreeze Chromogenic Kit from Life Technologies, or AMRESCO, Solon, OH) for subsequent chromogenic detection. Developed Western blots were imaged with an Epson Perfection V700 Photo scanner and quantified with ImageJ.

Microtubule gliding assays

As described in previous work (29,30), microtubule gliding assays were performed in 5 μL flow channels made from an 18 × 18 mm cover slip (Corning B.V. Life Sciences, Amsterdam, Netherlands) spaced ~100 μm from a 20 × 20 mm cover slip (Corning) or microscope slide (Corning) by Parafilm M (Pechiney Plastic Packaging, Chicago, IL). The flow channels were filled sequentially with the following solutions: 20 μL HMDE; 10 μL 1 mg/mL biotinylated bovine serum albumin (BSA); 20 μL HMDE; 10 μL 1 mg/mL streptavidin; 20 μL HMDE; 10 μL 5 mg/mL BSA; 20 μL HMDE; 10 μL 100 μg/mL axonemal dynein; 20 μL HMDE with 1 mM ADP; 10 μL microtubule solution (0.5 μM microtubules, 20 μM taxol, and 1 mM ADP in HMDE); 20 μL HMDE with 1 mM ADP and 20 μM taxol; and 10 μL motility solution (1 mM ATP, 1 mM ADP, 20 μM taxol, 4 μg/mL catalase, 10 μg/mL glucose oxidase, 20 mM D-glucose, and 1% β-mercaptoethanol in HMDE). Note that solutions subsequently imaged in dark field were centrifuged in an Airfuge before use and the catalase, glucose oxidase and D-glucose were omitted from the motility solution. All solutions containing protein were incubated in the flow channel for 5 min.

Rhodamine-labeled porcine microtubules were imaged translocating using a Zeiss Axiovert 200M microscope with a Zeiss 100×/1.46 a-Plan-Apochromat Oil Ph3, Plan-NeoFlaur 40×/1.3, or Plan ApoChromat 63×/1.4 Ph water objective at 23°C. Alternatively, unlabeled *Chlamydomonas* microtubules were imaged using a Plan-NeoFluar 100×/1.3 objective with iris and a Zeiss dark field oil condenser/1.3. Images were acquired with a Metamorph (Molecular Devices, Sunnyvale, CA) or Andor iQ (Andor TechTology, Belfast, UK) software-driven Andor DV887 iXon camera. The exposure time was 100 ms, and 2000 frame movies were recorded continuously.

In each movie, microtubules were tracked with 50 nm precision, and the displacement along the microtubule's path and the microtubule's length were calculated in every frame using Fluorescence Image Evaluation Software for Tracking and Analysis (FIESTA) (38). The instantaneous velocity of the microtubule was calculated over 0.4 s intervals after smoothing the data with a third-degree Savitzky-Golay filter with a span of nine data points (29,30). The displacement-weighted mean velocities were calculated as described in Alper et al. 2013 (29) by binning the instantaneous velocities in 200 nm/s bins. Displacement-weighted mean velocity data plotted against microtubule length were weighted by the total tracked displacement and fitted to the Mechaelis-Menten-like equation (Eq. 1) using the Levenberg-Marquardt method of calculating a nonlinear least squares regression in MATLAB (The MathWorks, Natick, MA).

All gliding assay data were collected using microtubules from at least two enzymatic treatments, each in at least two flow channels, and from one to three movies from each flow channel. The reported data were pooled based on the lack of statistical significance of any differences between movies from the same experimental conditions.

RESULTS

To determine whether axonemal dyneins sense tubulin modifications, we studied two classes of modifications: α-tubulin K40 acetylation and those localized to the CTTs. We treated microtubules in vitro to alter the state of either of these groups, and we tested the effect on purified axonemal dynein in reconstituted in vitro motility assays.

αTAT treatment acetylates porcine microtubules

We incubated porcine-brain microtubules with recombinant mouse αTAT (10,11), which transfers the acetyl group from acetyl-CoA to the epsilon amine of α-tubulin K40 (Fig. 1 *A*). Using an antiacetylated-K40 antibody (39), we found that αTAT-treated microtubules were more heavily acetylated than untreated microtubules (Fig. 1 *B*). αTAT treatment did not affect polyglutamylation, detyrosination, or Δ2 generation, which is the irreversible cleavage of the C-terminal glutamic acid and tyrosine from α-tubulin (2) (Fig. 1 *B*).

Increased αTAT incubation time increases the amount of porcine tubulin that is acetylated

To determine the effect of porcine microtubule K40 acetylation on axonemal dynein motility, we generated increasingly acetylated microtubules by treating microtubules with αTAT for increasing periods. We found that the amount of acetylation increased with increasing αTAT exposure time (Fig. 1 *C*). We quantified the Western blot by densitometry and found that acetylation saturated to a level ~15-fold over untreated microtubules after 60 min of αTAT treatment (Fig. 1 *D*).

Acetylation increases the speed of axonemal dynein on porcine brain microtubules

We performed in vitro gliding assays using the increasingly acetylated porcine brain microtubules to determine if acetylation affects the motility of axonemal outer arm axonemal dynein purified from *Chlamydomonas*. Using fluorescence microscopy, we recorded movies of the rhodamine-labeled porcine microtubules gliding on axonemal dynein-coated slides and tracked each microtubule's path in the movies. Because the gliding motility was unsteady, as is typical for axonemal dyneins (see Fig. 1 *E* for a typical example) (29,31,40), we calculated the mean velocity of each microtubule track using displacement-weighted velocity analysis (29). We plotted the displacement-weighted mean velocity (v) against the microtubule length (L) for each condition (see Fig. 1 *F* for an example condition) and fit these data with the following Michaelis-Menten-like equation (29,40) using nonlinear regression (see Materials and Methods):

$$v(L) = v_{\max}\frac{L}{L_0 + L}, \quad (1)$$

where $v_{\max}$ is the displacement-weighted mean velocity reached in the limit of long microtubules (Fig. 1 *F*), and L_0 is the length of the microtubule with gliding velocity $v_{\max}/2$ (Fig. 1 *F*). The fit curve was not significantly different from the data ($\chi^2 = 12.0$, $df = 9$, $p = 0.21$). We tested an extension of Eq. 1 by adding a constant.

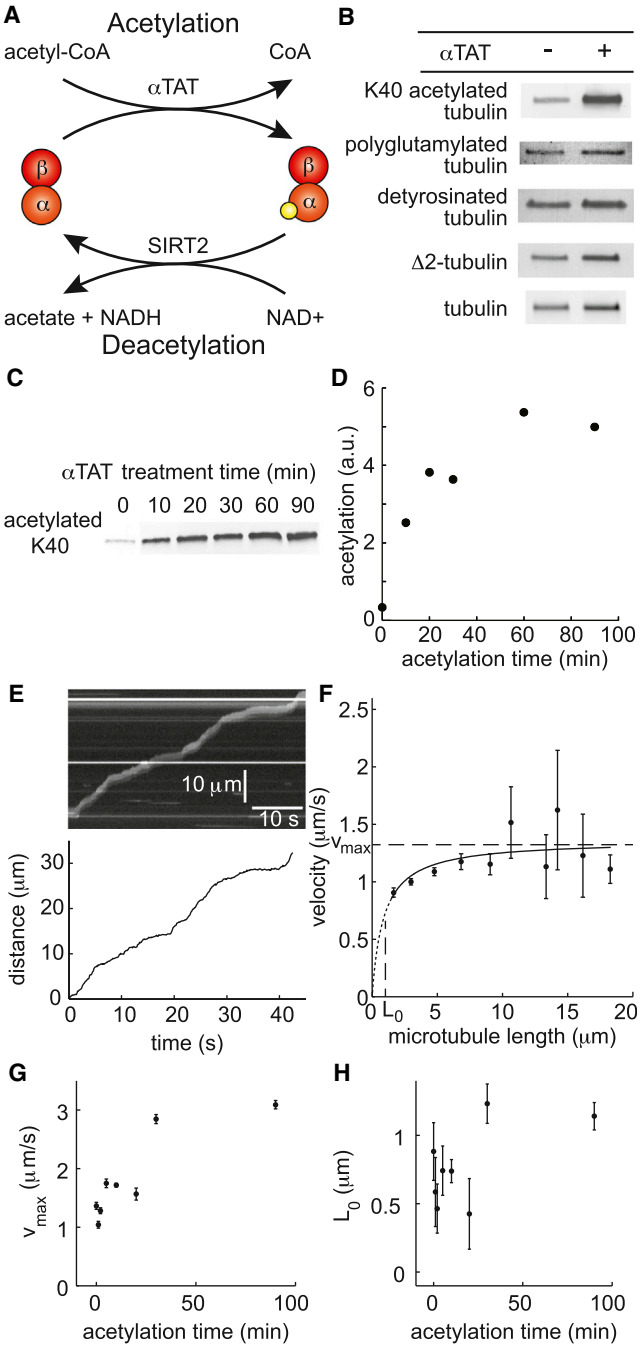

FIGURE 1 Increasing acetylation increases axonemal dynein speed on porcine microtubules. (*A*) Schematic of tubulin acetylation and deacetylation by αTAT and SIRT2, respectively. The orange and red circles represent α- and β-tubulins, respectively. The yellow circle represents the acetylated form of K40. (*B*) Western blots of porcine microtubules treated with αTAT showing that αTAT treatment significantly increased the fraction of acetylated tubulin whereas the CTT-associated PTMs were unaffected. Tubulin loading was assayed by visualization in the gel using the TGX Stain-Free Precast Gel protocol before transfer to the nitrocellulose membrane. (*C*) Western blot of microtubules treated with αTAT showing that increased αTAT treatment time increases the fraction of acetylated tubulin. (*D*) Densitometry of the Western blot from panel *C*. (*E*) Example raw gliding assay data. (*top*) Typical kymograph of a microtubule (length = 2.6 μm) gliding on axonemal dynein that shows the characteristic unsteadiness of axonemal dynein gliding assays. (*bottom*) Plot of the microtubule's distance traveled as a function of time. This is an example of typical gliding data after tracking. (*F*) Typical plot of mean microtubule gliding velocity as a function of microtubule length. This example is for the case of untreated microtubules. The data points were calculated by pooling microtubules in 2 μm bins and averaging their displacement-weighted mean velocities. The error bars are the standard error of the mean for each bin. The line is a least squares fit to Eq. 1 calculated before pooling and weighted by total distance traveled. This fit was used to calculate v_{max} and L_0, shown with dashed lines, and it is typical of all cases. (*G*) The calculated v_{max} for each αTAT treatment condition plotted as a function of acetylation time. (*H*) The calculated L_0 for each αTAT treatment condition plotted as a function of acetylation time. The data points for panels *G* and *H* were calculated by pooling the microtubule tracks from at least three movies per condition. A total of 213, 140, 280, 257, 1034, 94, 474, and 438 microtubules were analyzed for the αTAT treatment times of 0, 1, 2, 5, 10, 20, 30, and 90 min, respectively. The error bars in *G* and *H* are the standard errors for each parameter. To see this figure in color, go online.

We found that the value of the constant was not significantly different from zero (Student's *t*-test, $t = 0.33$, $df = 7$, $p = 0.82$), indicating that adding a constant does not increase the goodness of fit. When we added cooperativity by raising all lengths to the power n (Hill coefficient), we found that n was not significantly different from one (Student's *t*-test, $t = 0.094$, $df = 7$, $p = 0.93$). This indicates that Eq. 1 provides a simple and satisfactory fit to the data. By contrast, a linear fit was significantly different from the data ($\chi^2 = 25.5$, $df = 9$, $p = 0.0024$).

We found that v_{max} increased with increasing αTAT acetylation time and that the effect on velocity saturated after 30 min of αTAT acetylation time to a value that was about threefold higher than untreated microtubules (Fig. 1 *G*). L_0 also increased with acetylation time (Fig. 1 *H*), but a linear regression indicated that this increase was not statistically significant (slope = 0.0059 ± 0.0032 μm/min, fit parameter ± *SE* of the fit, $t = 1.84$, $df = 6$, $p = 0.12$). We will discuss the implications of the increase in v_{max} and the lack of a statistically significant change in L_0 on the motility properties of molecular axonemal dynein in the Discussion section.

SIRT2 treatment deacetylates *Chlamydomonas* axonemal tubulin

To further investigate the effects of acetylation on the motility of axonemal dynein, we deacetylated purified *Chlamydomonas* axonemal tubulin, which is strongly K40-acetylated in vivo (39,41), using recombinant human SIRT2 to remove the acetyl group from K40 (Fig. 1 *A*) (12). We found that SIRT2-treated tubulin was much less acetylated than untreated tubulin (Fig. 2 *A*). Additionally, we confirmed that SIRT2 treatment did not affect the polyglutamylation, detyrosination, or Δ2 generation of *Chlamydomonas* tubulin (Fig. 2 *A*).

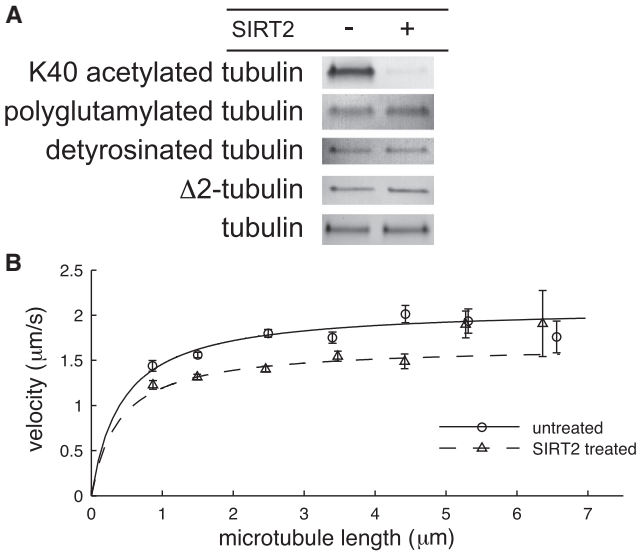

FIGURE 2 Deacetylation decreased axonemal dynein speed on *Chlamydomonas* microtubules. (*A*) Western blots of *Chlamydomonas* microtubules treated with SIRT2 showing that ΣIPT2 treatment significantly decreased the fraction of acetylated tubulin whereas other CTT-associated PTMs were unaffected. Tubulin loading was assayed by visualization in the gel using the TGX Stain-Free Precast Gel protocol before transfer to the nitrocellulose membrane. (*B*) The mean velocity of SIRT2-treated (*triangles*) and untreated (*circles*) microtubules plotted as a function of microtubule length. The data points were calculated by pooling microtubules in 1 μm bins and averaging their displacement-weighted velocities. The error bars are the standard error of the mean for each microtubule bin. The lines, which are least-squares fits to Eq. 1 for the unpooled SIRT2-treated (*dashed*) and untreated (*solid*) microtubules, respectively, were calculated before pooling and weighted by total distance traveled.

Deacetylation decreases the speed of axonemal dynein on *Chlamydomonas* microtubules

We performed in vitro gliding assays to determine if deacetylation of *Chlamydomonas* microtubules affects the motility of axonemal dynein. Using dark field microscopy to record movies of gliding unlabeled *Chlamydomonas* microtubules and by fitting the tracked data to Eq. 1, we found that deacetylation decreased the v_{max} by 20%, from 2.09 ± 0.06 μm/s for untreated microtubules to 1.66 ± 0.06 μm/s for SIRT2-treated microtubules (v_{max} ± *SE* of the fit, N = 613 and 538 microtubule tracks, respectively). Though the effect was subtle, the decrease in velocity was statistically significant ($p < 0.001$, Student's *t*-test, see Fig. 2 *B*). We found that deacetylation slightly decreased L_0, from 0.43 ± 0.08 μm for untreated microtubules to 0.39 ± 0.08 μm for SIRT2-treated microtubules (L_0 ± *SE* of the fit, N = 613 and 538 microtubule tracks, respectively, Fig. 2 *B*), but not significantly so ($p > 0.5$, Student's *t*-test).

There is no statistical significance in the differences between deacetylated and control microtubules with $L >$ 5 μm (Fig. 2 *B*, two-sample *t*-tests, for the 5.5 μm data point: $t = 0.14$, $df = 29$, $p = 0.89$; for the 6.5 μm data point: $t = 0.38$, $df = 14$, $p = 0.71$); however, this is because of the small number of tracked microtubules of these lengths. *t*-tests on the deacetylated data points for $L > 5$ μm show that these data points are not statistically different from the fit line (for the 5.5 μm data point: $t = 1.85$, $df = 6$, $p = 0.11$; for the 6.5 μm data point: $t = 0.68$, $df = 5$, $p = 0.53$). Therefore, despite the lack of difference between the deacetylated and control microtubules with $L > 5$ um, there is strong, statistically significant evidence that long deacetylated microtubules are slower than control ones, because, when all the data is included in the fit, v_{max} is significantly lower for deacetylated microtubules than for control ones.

Subtilisin cleaves off the C-terminal tails and the removes CTT-related posttranslational modifications from porcine microtubules

To test the effects of the C-terminal tails and CTT-related PTMs on axonemal dynein's motility, we removed the 2-4 kDa CTTs, including the associated posttranslational modifications, from porcine microtubules in vitro using the subtilisin A protease (Fig. 3 *A*). Because α- and β-tubulin CTTs are differently susceptible to subtilisin treatment (19), we treated polymerized microtubules with 200 μg/mL, 10 μg/mL, and 0 μg/mL (as a control) of subtilisin. We found that digestion by 10 μg/mL of subtilisin increased the mobility of one tubulin in SDS-PAGE: one of the Coomassie brilliant blue-stained bands migrated farther, with lower apparent molecular weight, than the other (Fig. 3 *B*, compare *lane 2* with *lane 1*). Neither anti-α-tubulin-CTTs nor anti-β-tubulin-CTTs stained the altered band in Western blots. Only anti-α-tubulin-CTTs stained the unchanged band (Fig. 3 *B*). We conclude that the 10 μg/mL subtilisin digestion cleaved the CTTs off β-tubulin leaving α- β_s-tubulin microtubules, where β_s-tubulin indicates the s-tubulin form of β-tubulin. Digestion with 200 μg/mL yielded the appearance of a second higher-mobility band and the disappearance of the lower-mobility band (Fig. 3 *B*, *lane 3*). Neither of the bands in lane 3 were stained by anti-α-tubulin-CTTs or anti-β-tubulin-CTTs in Western blots (Fig. 3 *B*). This indicated that the 200 μg/mL subtilisin digestion cleaved the CTTs off both α- and β-tubulin leaving α_s- β_s-tubulin microtubules. The 200 μg/mL subtilisin digestion left no detectable CTTs on α- or β-tubulin in the microtubules (Fig. 3 *B*).

We confirmed that subtilisin treatment removed CTT-related posttranslational modifications with several antibodies. Polyglutamylation, detyrosination, and Δ2 generation were eliminated from β-tubulin with 10 μg/mL and from both α- and β-tubulin with 200 μg/mL subtilisin treatments (Fig. 3 *C*). However, the anti-K40 acetylated tubulin antibody stained the control and both treatments (Fig. 3 *C*).

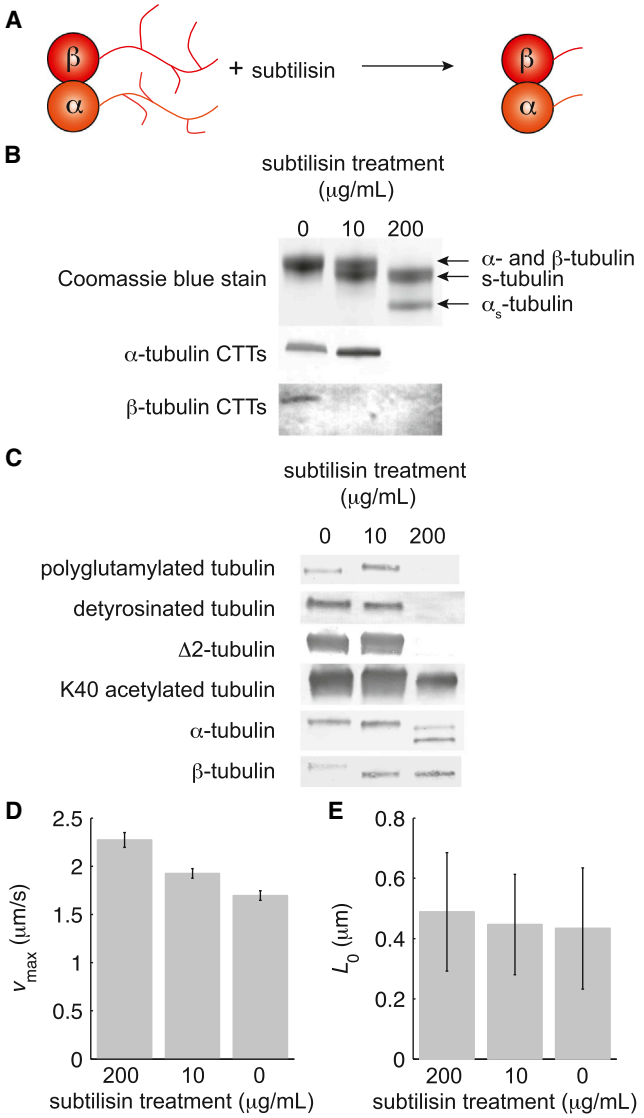

FIGURE 3 CTT cleavage increases axonemal dynein speed on porcine microtubules. (*A*) Schematic of CTT cleavage by subtilisin. The orange and red circles represent α- and β-tubulins, respectively. The orange and red branched lines represent α- and β-tubulin CTTs with their CTT-related PTMs, respectively. (*B*) Gel electrophoresis of subtilisin-treated porcine microtubules stained with Coomassie brilliant blue. The bands are identified with arrows. α-tubulin and β-tubulin CTTs were visualized in these Western blots with CTT-specific antibodies. (*C*) Western blots of porcine microtubules treated with subtilisin showing that CTT-related posttranslational modifications were cleaved by treatment, whereas K40 acetylation remained in all treatments. α- and β-tubulins were visualized with antibodies that recognize epitopes not in their CTTs. (*D*) The calculated v_{max} for axonemal dynein on α- β-tubulin microtubules (0 μg/mL), α- β_s-tubulin microtubules (10 μg/mL), and α_s- β_s-tubulin microtubules (200 μg/mL). (*E*) The calculated L_0 for each subtilisin treatment. The data reported in both *D* and *E* were the fit parameters from a nonlinear least squares regression of 392, 711, and 712 microtubule tracks from subtilisin incubation concentrations of 200, 10, and 0 μg/mL, respectively. The error bars are the standard errors of the regression for each parameter. To see this figure in color, go online.

Cleavage of CTTs increases the speed of axonemal dynein

We performed in vitro gliding assays to determine how CTTs, and the posttranslational modifications that localize to CTTs, affect the motility of axonemal dynein. We analyzed the motility as we had done for acetylated microtubules above. We found that cleavage of β-tubulin CTTs from porcine microtubules increased v_{max} by ~15%, from 1.70 ± 0.05 μm/s for untreated microtubules to 1.93 ± 0.05 μm/s for 10 μg/mL subtilisin-treated microtubules (v_{max} ± *SE* of the fit, $N = 712$ and 711 microtubule tracks, respectively, Fig. 3 *D*). Cleavage of both α- and β-tubulin CTTs with the 200 μg/mL subtilisin treatment increased v_{max} by ~35%, from 1.70 ± 0.05 μm/s for untreated microtubules to 2.27 ± 0.07 μm/s for 200 μg/mL subtilisin-treated microtubules (v_{max} ± *SE* of the fit, $N = 712$ and 392 microtubule tracks, respectively, Fig. 3 *D*). The values of v_{max} were significantly different from each other and from untreated microtubules ($p < 0.001$ in all cases, Student's *t*-test). We found that CTTs did not have a significant effect on L_0 (Fig. 3 *E*, $p > 0.5$ in both cases, Student's *t*-test).

DISCUSSION

Acetylation regulates the motility of outer arm axonemal dynein

We found that the speed of *Chlamydomonas* outer arm axonemal dynein on mammalian microtubules increased up to threefold after acetylation with αTAT (Fig. 1 *G*). Thus, the reduced motility of sperm in αTAT knockout mice (21) may be because of a direct effect on axonemal dynein. We also found a small effect on the motility of axonemal dynein on *Chlamydomonas* microtubules deacetylated by SIRT2 consistent with the small reduction of swimming speed in *Chlamydomonas* cells with reduced acetylation (20). Therefore, our results support the hypothesis that acetylation regulates the ciliary beat through a direct modulation of axonemal dynein-microtubule interactions.

Our results have interesting implications regarding inside-out signaling across the microtubule wall. K40 is located on the inner, luminal surface of the microtubule (42,43), yet its acetylation regulates the motility of the axoneme, which ultimately involves the interactions between axonemal dynein and the outer surface of the microtubule. Likewise, microtubule-inner proteins, MIPs, are also implicated in the regulation of the ciliary beat (44). These findings suggest that there is a communication pathway through the microtubule wall in cilia. However, there is scant biochemical evidence for a direct effect of acetylation on motility. Reed et al. found that intact axonemes from a *Tetrahymena* mutant that lacks K40 acetylation (α-tubulin K40R) are moved more slowly by kinesin-1 than axonemes

from wildtype cells (7) despite the α-tubulin K40R mutation leading to no significant difference in *Tetrahymena* swimming velocity (22). It is possible that the effect is indirect. For example, the lack of acetylation may disrupt microtubule assembly within the axoneme leading to structural differences on the outer surface that affect kinesin-1, rather than the acetylation itself directly regulating the kinesin-1 activity. Consistent with this possibility, acetylation of mammalian brain microtubules has no effect on kinesin-1 in vitro motility (13,14). By contrast, our results with outer arm axonemal dynein and brain microtubules show a clear, strong effect of in vitro acetylation on motility. Although our results are consistent with inside-out signaling, a potential caveat is that αTAT may acetylate lysines located on the outer surface of the microtubule (4,45), which in turn regulate outer arm axonemal dynein motility. However, αTAT is thought to be specific for K40 (10). Thus, it is likely that acetylation of K40 can be sensed by outer arm axonemal dynein.

We favor a model in which acetylation of K40 leads to an allosteric conformational change across the microtubule wall to the site where axonemal dynein binds, some 5.5 nm away (46). Although no such conformational change was detected in a recent EM study comparing acetylated and deacetylated microtubules (47), the resolution (~8.5 Å) may not have been sufficient to detect an allosteric effect. An alternative to the allosteric model is that axonemal dynein residues reach through the microtubule fenestrations to interact directly with K40 (48). However, this is unlikely given that axonemal dynein's microtubule-binding domain binds to the microtubule at the intradimer α-tubulin-β-tubulin interface whereas K40 is located below the interdimer α-tubulin-β-tubulin interface (46,48).

Microtubule acetylation decreases the bound time of axonemal dynein

To elucidate the mechanism by which K40 acetylation regulates axonemal dynein, we mathematically modeled the gliding-assay results using a two-state model (29) for the axonemal dynein motors. The two-state model assumes that an axonemal dynein molecule moves a microtubule through the power stroke distance, δ, in the time it is bound, t_{bound}, to the microtubule. The model assumes that axonemal dynein has no effect on the microtubule in the time it is unbound, t_{unbound}. Axonemal dynein transitions from the bound to unbound state with a dissociation rate, $k_{\text{off}} = 1/t_{\text{bound}}$, and from the unbound to the bound state with an association rate, $k_{\text{on}} = 1/t_{\text{unbound}}$. This model is quite different from that used to describe processive motors such as kinesin-1 and cytoplasmic dynein, which take many steps while bound to the filament (49): in this case the binding to and unbinding from the filament can be separated from the stepping mechanism. Outer arm axonemal dynein spends only a small fraction of its time in the bound state (40); therefore, the following duty ratio is small:

$$r = \frac{t_{bound}}{t_{bound} + t_{unbound}}. \quad (2)$$

In gliding assays, if the motor density on the surface (ρ) or the microtubule length (L) is great enough so that many motors are under the microtubule ($N = \rho L$, $[1\text{-}r]^N << 1$), then, at any one time, there will be at least one axonemal dynein in the bound state and hence the microtubule gliding speed (v) will be equal to the power stroke speed, v_0, where

$$v_0 = \frac{\delta}{t_{bound}}. \quad (3)$$

Thus, the higher speed of long acetylated microtubules (v_{max}) suggests that acetylation either increases the power stroke distance or decreases the bound time (Eq. 3) of axonemal dynein. The power stroke distance is likely to be a property of axonemal dynein alone (independent of the axonemal dynein-microtubule interaction) given that the current mechanical model of axonemal dynein's power stroke mechanism predicts that step size is determined by axonemal dynein tail-AAA+ ring linker rearrangements and AAA+ ring rotations (50). Therefore, we propose that acetylation decreases the bound time, t_{bound}, i.e., it increases (by about threefold) the dissociation rate of axonemal dynein from the microtubule, k_{off}.

The CTT has a modest effect on outer arm axonemal dynein motility

We found that removal of the CTT, and therefore removal of the associated PTMs, leads to a modest increase in the speed of outer arm axonemal dynein. Therefore, using the same reasoning as for acetylation, CTTs decrease axonemal dynein's k_{off}, although to a lesser magnitude than acetylation's effect. This subtle in vitro effect is in general agreement with in vivo studies, even though CTT-related PTMs tend to have a more pronounced effect on motility (24,25,27,28) than acetylation does (20,22). The reason for the agreement is that CTT-related PTMs, particularly polyglutamylation, have a stronger effect on inner arm axonemal dynein than outer arm axonemal dynein motility (24–26). Additionally, CTT-related PTMs have competing effects on the motility of cytoplasmic motors, e.g., detyrosination inhibits kinesin-2 whereas polyglutamylation increases its motility (15). Moreover, the sign of the impact on gliding velocity, v_{max}, is consistent with previous studies showing that polyglutamylation tends to inhibit axonemal dynein sliding motility (24,26). Finally, our results show that outer arm axonemal dynein and cytoplasmic dynein, which is not affected by changing tubulin CTTs (15), are differently regulated by the tubulin in microtubules.

There are multiple mechanisms by which CTTs might decrease axonemal dynein speed. Because CTTs are located on the outer surface of microtubules (43) and can be quite large, particularly if they are heavily modified with polymodifications (2), they may directly interact with or even sterically hinder axonemal dynein. Additionally, because they are glutamic acid rich and thus negatively charged, CTTs might electrostatically interact with the positively charged microtubule-binding domains of axonemal dynein (26). A simple potential mechanism is that the CTT facilitates axonemal dynein-microtubule binding by decreasing the off-rate, leading to a lower speed.

Acetylation and CTTs do not have a significant effect on the duty ratio of axonemal dynein

At intermediate microtubule lengths, we expect the gliding velocity to depend on length (29,40) as in the following:

$$v = v_0\left[1-(1-r)^{\rho L}\right] \cong v_{\max}\frac{L}{L_0+L}, \quad (4)$$

where

$$L_0 \cong \frac{\ln(2)}{\rho r}, \quad (5)$$

for small r (29). According to Eq. 5, the lack of statistical significance of the change in L_0 indicates that the duty ratio, r, of axonemal dynein is unaffected by both K40 acetylation and CTTs. Therefore, in light of Eq. 2, the finding that r is unchanged implies that acetylation increases k_{on} threefold and CTTs decrease k_{on} 35% (because k_{off} was increased threefold by acetylation and decreased 35% by CTTs). However, the effects of acetylation and CTTs on L_0 have a large uncertainty. The 95% confidence interval for the slope of the linear fit to Fig. 1 *H* was -0.002 to 0.014 μm/min. At the upper end of the interval, the change in L_0 predicts r could have been reduced by as much as twofold by acetylation; in this case, acetylation could have increased k_{on} as little as 1.5-fold. Thus, we estimate that acetylation increases k_{on} somewhere between 1.5-fold and threefold. More detailed structural, biophysical, and biochemical experiments will be necessary to reveal the mechanism by which it does this.

CONCLUSIONS

This study provides direct in vitro evidence of acetylation and CTTs regulating the motility of axonemal dynein. It suggests that cells can modify the tubulin to tune it specifically for optimal use in cilia. This model for motor protein regulation has implications beyond ciliary motility, and it further strengthens the argument that PTMs of tubulin help specify the tubulin code by differentially regulating motor protein activity.

The authors thank Natalia Szydlowska, Barbara Borgonovo, and David Drechsel for advice on, and help with, purifying the proteins, and the entire Howard lab for fruitful discussions, various reagents, and careful reading of the manuscript. We thank the Howard lab tubulin prep team for the porcine brain tubulin. We very much appreciate the kind gift of the *Chlamydomonas oda2-t-lc2-bccp* strain from Ritsu Kamiya and the αTAT from Stefan Diez.

This work was supported by funding from the Max Planck Society, the European Community as part of a Marie Curie Incoming International Fellowship Grant No. 276217, and Yale University.

REFERENCES

1. Verhey, K. J., and J. Gaertig. 2007. The tubulin code. *Cell Cycle.* 6:2152–2160.
2. Ludueña, R. F. 1998. Multiple forms of tubulin: different gene products and covalent modifications. *Int. Rev. Cytol.* 178:207–275.
3. Garnham, C. P., and A. Roll-Mecak. 2012. The chemical complexity of cellular microtubules: tubulin post-translational modification enzymes and their roles in tuning microtubule functions. *Cytoskeleton.* 69:442–463.
4. Janke, C., and J. C. Bulinski. 2011. Post-translational regulation of the microtubule cytoskeleton: mechanisms and functions. *Nat. Rev. Mol. Cell Biol.* 12:773–786.
5. Dompierre, J. P., J. D. Godin, …, F. Saudou. 2007. Histone deacetylase 6 inhibition compensates for the transport deficit in Huntington's disease by increasing tubulin acetylation. *J. Neurosci.* 27:3571–3583.
6. Cai, D., D. P. McEwen, …, K. J. Verhey. 2009. Single molecule imaging reveals differences in microtubule track selection between Kinesin motors. *PLoS Biol.* 7:e1000216.
7. Reed, N. A., D. Cai, …, K. J. Verhey. 2006. Microtubule acetylation promotes kinesin-1 binding and transport. *Curr. Biol.* 16:2166–2172.
8. Hammond, J. W., C.-F. Huang, …, K. J. Verhey. 2010. Posttranslational modifications of tubulin and the polarized transport of kinesin-1 in neurons. *Mol. Biol. Cell.* 21:572–583.
9. Neumann, B., and M. A. Hilliard. 2014. Loss of MEC-17 leads to microtubule instability and axonal degeneration. *Cell Reports.* 6:93–103.
10. Akella, J. S., D. Wloga, …, J. Gaertig. 2010. MEC-17 is an α-tubulin acetyltransferase. *Nature.* 467:218–222.
11. Shida, T., J. G. Cueva, …, M. V. Nachury. 2010. The major α-tubulin K40 acetyltransferase alphaTAT1 promotes rapid ciliogenesis and efficient mechanosensation. *Proc. Natl. Acad. Sci. USA.* 107:21517–21522.
12. North, B. J., B. L. Marshall, …, E. Verdin. 2003. The human Sir2 ortholog, SIRT2, is an NAD+-dependent tubulin deacetylase. *Mol. Cell.* 11:437–444.
13. Walter, W. J., V. Beránek, …, S. Diez. 2012. Tubulin acetylation alone does not affect kinesin-1 velocity and run length in vitro. *PLoS ONE.* 7:e42218.
14. Kaul, N., V. Soppina, and K. J. Verhey. 2014. Effects of α-tubulin K40 acetylation and detyrosination on kinesin-1 motility in a purified system. *Biophys. J.* 106:2636–2643.
15. Sirajuddin, M., L. M. Rice, and R. D. Vale. 2014. Regulation of microtubule motors by tubulin isotypes and post-translational modifications. *Nat. Cell Biol.* 16:335–344.
16. Wang, Z., and M. P. Sheetz. 2000. The C-terminus of tubulin increases cytoplasmic dynein and kinesin processivity. *Biophys. J.* 78:1955–1964.
17. Skiniotis, G., J. C. Cochran, …, A. Hoenger. 2004. Modulation of kinesin binding by the C-termini of tubulin. *EMBO J.* 23:989–999.
18. Lakämper, S., and E. Meyhöfer. 2005. The E-hook of tubulin interacts with kinesin's head to increase processivity and speed. *Biophys. J.* 89:3223–3234.

19. Hertzer, K. M., and C. E. Walczak. 2008. The C-termini of tubulin and the specific geometry of tubulin substrates influence the depolymerization activity of MCAK. *Cell Cycle.* 7:2727–2737.

20. Kozminski, K. G., D. R. Diener, and J. L. Rosenbaum. 1993. High level expression of nonacetylatable α-tubulin in *Chlamydomonas reinhardtii*. *Cell Motil. Cytoskeleton.* 25:158–170.

21. Kalebic, N., S. Sorrentino, …, P. A. Heppenstall. 2013. αTAT1 is the major α-tubulin acetyltransferase in mice. *Nat. Commun.* 4:1962.

22. Gaertig, J., M. A. Cruz, …, M. A. Gorovsky. 1995. Acetylation of lysine 40 in alpha-tubulin is not essential in Tetrahymena thermophila. *J. Cell Biol.* 129:1301–1310.

23. Janke, C., K. Rogowski, …, B. Eddé. 2005. Tubulin polyglutamylase enzymes are members of the TTL domain protein family. *Science.* 308:1758–1762.

24. Suryavanshi, S., B. Eddé, …, J. Gaertig. 2010. Tubulin glutamylation regulates ciliary motility by altering inner dynein arm activity. *Curr. Biol.* 20:435–440.

25. Kubo, T., H. A. Yanagisawa, …, R. Kamiya. 2010. Tubulin polyglutamylation regulates axonemal motility by modulating activities of inner-arm dyneins. *Curr. Biol.* 20:441–445.

26. Kubo, T., T. Yagi, and R. Kamiya. 2012. Tubulin polyglutamylation regulates flagellar motility by controlling a specific inner-arm dynein that interacts with the dynein regulatory complex. *Cytoskeleton.* 69:1059–1068.

27. van Dijk, J., K. Rogowski, …, C. Janke. 2007. A targeted multienzyme mechanism for selective microtubule polyglutamylation. *Mol. Cell.* 26:437–448.

28. Vent, J., T. A. Wyatt, …, R. Hallworth. 2005. Direct involvement of the isotype-specific C-terminus of beta tubulin in ciliary beating. *J. Cell Sci.* 118:4333–4341.

29. Alper, J. D., M. Tovar, and J. Howard. 2013. Displacement-weighted velocity analysis of gliding assays reveals that *Chlamydomonas* axonemal dynein preferentially moves conspecific microtubules. *Biophys. J.* 104:1989–1998.

30. Alper, J., V. Geyer, …, J. Howard. 2013. Reconstitution of flagellar sliding. *In* Methods in Enzymology. W. F. Marshall, editor. Academic Press, Burlington, MA, pp. 343–369.

31. Furuta, A., T. Yagi, …, R. Kamiya. 2009. Systematic comparison of in vitro motile properties between *Chlamydomonas* wild-type and mutant outer arm dyneins each lacking one of the three heavy chains. *J. Biol. Chem.* 284:5927–5935.

32. Brokaw, C. J., and R. Kamiya. 1987. Bending patterns of *Chlamydomonas* flagella: IV. Mutants with defects in inner and outer dynein arms indicate differences in dynein arm function. *Cell Motil. Cytoskeleton.* 8:68–75.

33. Gorman, D. S., and R. P. Levine. 1965. Cytochrome f and plastocyanin: their sequence in the photosynthetic electron transport chain of *Chlamydomonas reinhardi*. *Proc. Natl. Acad. Sci. USA.* 54:1665–1669.

34. Witman, G. 1986. Isolation of *Chlamydomonas* flagella and flagellar axonemes. *Methods in Enzymology.* 134:280–290.

35. Kagami, O., and R. Kamiya. 1992. Translocation and rotation of microtubules caused by multiple species of *Chlamydomonas* inner-arm dynein. *J. Cell Sci.* 103:653–664.

36. Gell, C., C. T. Friel, …, J. Howard. 2011. Purification of tubulin from porcine brain. *In* Methods in Molecular Biology. Springer, Totowa, NJ.

37. Widlund, P. O., M. Podolski, …, D. N. Drechsel. 2012. One-step purification of assembly-competent tubulin from diverse eukaryotic sources. *Mol. Biol. Cell.* 23:4393–4401.

38. Ruhnow, F., D. Zwicker, and S. Diez. 2011. Tracking single particles and elongated filaments with nanometer precision. *Biophys. J.* 100:2820–2828.

39. Piperno, G., and M. T. Fuller. 1985. Monoclonal antibodies specific for an acetylated form of alpha-tubulin recognize the antigen in cilia and flagella from a variety of organisms. *J. Cell Biol.* 101:2085–2094.

40. Hamasaki, T., M. E. Holwill, …, P. Satir. 1995. Mechanochemical aspects of axonemal dynein activity studied by in vitro microtubule translocation. *Biophys. J.* 69:2569–2579.

41. L'Hernault, S. W., and J. L. Rosenbaum. 1985. Chlamydomonas .alpha.-tubulin is posttranslationally modified by acetylation on the .epsilon.-amino group of a lysine. *Biochemistry.* 24:473–478.

42. Soppina, V., J. F. Herbstman, …, K. J. Verhey. 2012. Luminal localization of α-tubulin K40 acetylation by cryo-EM analysis of fab-labeled microtubules. *PLoS ONE.* 7:e48204.

43. Nogales, E., M. Whittaker, …, K. H. Downing. 1999. High-resolution model of the microtubule. *Cell.* 96:79–88.

44. Nicastro, D., X. Fu, …, R. W. Linck. 2011. Cryo-electron tomography reveals conserved features of doublet microtubules in flagella. *Proc. Natl. Acad. Sci. USA.* 108:E845–E853.

45. Choudhary, C., C. Kumar, …, M. Mann. 2009. Lysine acetylation targets protein complexes and co-regulates major cellular functions. *Science.* 325:834–840.

46. Redwine, W. B., R. Hernández-López, …, A. E. Leschziner. 2012. Structural basis for microtubule binding and release by dynein. *Science.* 337:1532–1536.

47. Howes, S. C., G. M. Alushin, …, E. Nogales. 2014. Effects of tubulin acetylation and tubulin acetyltransferase binding on microtubule structure. *Mol. Biol. Cell.* 25:257–266.

48. Yajima, H., T. Ogura, …, N. Hirokawa. 2012. Conformational changes in tubulin in GMPCPP and GDP-taxol microtubules observed by cryoelectron microscopy. *J. Cell Biol.* 198:315–322.

49. Howard, J. 2001. Mechanics of Motor Proteins and the Cytoskeleton. Sinauer Associates, Sunderland, MA.

50. Lin, J., K. Okada, …, D. Nicastro. 2014. Structural mechanism of the dynein power stroke. *Nat. Cell Biol.* 16:479–485.